The viability of reflection loss measurement inversion to predict broadband acoustic behavior

Marcia J. Isakson[a)]
Applied Research Laboratories, The University of Texas at Austin, Austin, Texas 78713-8029

Tracianne B. Neilsen
Department of Physics and Astronomy, Brigham Young University, Provo, Utah 84602

(Received 18 March 2006; accepted 27 April 2006)

The viability of using reflection loss measurements for the determination of sediment parameters and the predictions of broadband acoustic behavior is studied as a function of frequency for a dispersive ocean bottom. For this study, a deterministic set of reflection loss values from an idealized dispersive sediment is calculated as a function of grazing angle over a large frequency band 100 Hz–1 MHz. In each of the four decades of frequency a simulated annealing optimization process is used to invert for the sediment parameters. In addition, a set of rotated coordinates is calculated that reveals the the relative sensitivities of the reflection data to each of the sediment parameters and therefore the ability of the inversion process to converge. The accuracy and precision of each estimate is analyzed. The predicted broadband acoustic behavior from the inverted parameters from each decade band was compared to the original model. Only the estimates obtained from data that include frequencies in the transition region can successfully predict broadband behavior. [DOI: 10.1121/1.2206515]

PACS number(s): 43.30.Pc, 43.20.Gp [WMC] Pages: 135–144

I. INTRODUCTION

The acoustic behavior of the ocean bottom can affect shallow-water transmission loss, reverberation estimation, ocean mapping, and acoustic communications. This behavior can be predicted by knowing the sediment parameters. Historically, ocean sediments have been characterized by five parameters: the compressional and shear sound speeds and attenuations and the density. However, recent data suggests that this parameterization is incomplete.[1–5] Current models such as the Biot-Stoll model,[6,7] the effective density fluid model,[8] and the Biot with contact squirt flow with shear drag model (BICSQS) (Ref. 9) require up to 13 parameters for complete characterization. Many of the parameters of these models are difficult if not impossible to measure. Additionally, current methods of sediment characterization are difficult, time consuming and invasive.[10]

Reflection loss measurements may provide a method of determining the parameter set for a poroelastic sediment which is both noninvasive and provides immediate results. In fact, there are several studies which attempt to use reflection loss measurements to predict sediment parameters in both a fluid and poroelastic framework.[11–15] However, many of these investigators use interrelations between the parameters or environmental measurements to estimate parameter values, rather than determining the parameters strictly from the data. For example, Holland[13] uses a form of the Kozeny-Carmen equation to estimate the value of the permeability based on the porosity. However, this method is only accurate for the case of well-sorted, unconsolidated sediments with roughly spherical grains.[16,17] In fact, for sandy sediments, the Kozeny-Carmen equation can overestimate permeability by an order of magnitude.[18]

In another study, Schock uses an inversion of normal reflection coefficient and attenuation measurements to obtain estimates of sediment parameters such as porosity, bulk density, permeability, and mean grain size.[15] However, Schock's method of determining the permeability requires the presence of a sub-bottom layer that is not always present. Also, the estimate for permeability assumes a frequency-independent value which has been challenged by Taylor-Smith, who demonstrated that permeability may vary up to an order of magnitude from the direct flow value.[19] Furthermore, Schock relies on interrelational expressions or measurements to determine the remaining poroelastic parameters. These expressions may not be valid. For example, his expression for the frame shear modulus is dependent on the total average stress and the porosity. However, as shown in the BICSQS model, the frame shear modulus may be dependent on the vicous drag of the interstitial fluid as well as the contact shear properties.[9]

It would be useful to devise a noninvasive method of determining the independent sediment parameters within a poroelastic framework from one measurement. The frequency- and angle-dependent reflection coefficient may provide a measurement set that can uniquely define all the parameters. The critical angle measurement is sensitive to the underlying sound speed, while the subcritical values are sensitive to shear speed and attenuation. Additionally, the normal reflection coefficient is sensitive to bulk density and porosity as shown by Schock.[15] However, there has been no detailed study to quantify the sensitivity of reflection coefficient loss measurements to poroelastic sediment parameters.

[a)]Electronic mail: misakson@arlut.utexas.edu

Also, since reflection loss has been shown to be frequency dependent, there have been no studies to quantify the ability of inversion results from one frequency band to predict the acoustic behavior over the broadband. The ability of one frequency band to predict the behavior of another band may be an important feature as high-frequency measurements are often easier to conduct.

The work presented herein contains a sensitivity study that strives to determine the viability of using estimates of seabed properties obtained from an inversion with angular- and frequency-dependent reflection coefficient data to predict broadband acoustic behavior. This study focuses on four features of the inversion. First, the relative sensitivity of each parameter is calculated. Second, the accuracy and precision of the inversion estimate is determined. Lastly, the parameter set from limited frequency ranges is used to predict broadband acoustic behavior.

It is understood that *in situ* measurements will be modified by interface roughness, volume inhomogeneity, range dependence, layering, and other experimental effects. However, the purpose of this work is to determine a baseline viability of the technique. In other words, given the complexity of the poroelastic model, are reflection coefficient measurements sensitive enough to provide estimates of sediment parameters?

The study was conducted using simulated data from 100 Hz to 1 MHz in four decade bands. The details of the simulated data calculation are given in Sec. II. The inversion methodology is described in Sec. III. Results are presented in Sec. IV and conclusion are made in Sec. V.

II. SIMULATED DATA

The simulated data are computed with the Biot-Stoll model. The data are computed for 50 frequencies on a logarithmic scale from 100 Hz to 1 MHz and for 180 angles from 1–90 deg. The Biot-Stoll formulation has been presented extensively in the literature[7] and is only summarized here. In Biot-Stoll theory, the equations are motion are governed by two coupled wave equations,

$$\nabla^2(He - C\zeta) = \frac{\partial^2}{\partial t^2}(\rho e - \rho_f \zeta), \tag{1}$$

$$\nabla^2(Ce - M\zeta) = \frac{\partial^2}{\partial t^2}(\rho_f e - m\zeta) - \frac{\eta}{\kappa}F(k)\frac{\partial \zeta}{\partial t}. \tag{2}$$

The fluid and frame move independently with displacements U and u, respectively. The volumetric strain is defined by $e=\mathrm{div}(u)$, and the local fluid content increase is $\zeta=\mathrm{div}(u-U)$. Equation (1) above describes the fluid and solid conservation, and Eq. (2) describes the fluid motion relative to the solid with two important first-order correction terms. The first term, $m\zeta$, describes the inertial coupling. This term is necessary at high frequencies since, according to Darcy's law, the fluid flow in the pores is not linearly related to the pressure gradient applied. In the Biot/Stoll formulation, m is given by $\tau\rho_f/\beta$, where τ is the tortuosity of the pores, ρ_f is the fluid density, and β is the porosity. The second correction term, $(\eta/\kappa)F(k)\ \partial\zeta/\partial t$, describes a coupling with viscosity η. Here, the fluid flow in the pores does not follow the Poiseuille law. Therefore, $F(k)$ is included to model the frequency dependence of viscous flow. The variable k is given by $a(\omega\rho_f/\eta)^{1/2}$, where a is the pore size parameter. The function, $F(k)$, approaches unity for low frequencies where the capillary flow can be modeled as parabolic. The moduli H, C, and M are derived by Stoll as[7]

$$H = \frac{(K_r - K_b)^2}{D - K_b} + K_b + \frac{4}{3}\mu, \tag{3}$$

$$C = \frac{K_r(K_r - K_b)}{D - K_b}, \tag{4}$$

$$M = \frac{K_r^2}{D - K_b}, \tag{5}$$

$$D = K_r\left[1 - \beta\left(\frac{K_r}{K_{f-1}}\right)\right]. \tag{6}$$

There are 13 independent parameters in the Biot-Stoll theory. The Biot parameters are generally grouped into three categories. The first category contains the bulk parameters: porosity β, fluid density ρ_f, fluid bulk modulus K_f, grain density ρ_g, and grain bulk modulus K_r. These parameters are generally well known and measurable. The fluid motion parameters form the next category: the viscosity η, the permeability κ, the pore size parameter a, and the tortuosity τ. These values are less well known and more difficult to measure. The last category is the frame response parameters: the frame shear modulus, $\tilde{\mu}=\mu+i\mu_i$, the frame bulk modulus, $\tilde{K}_b=K_b+iK_{b,i}$. These properties are not known and are practically impossible to measure directly.

A. Parameter bounds

It is necessary to determine realistic bounds for each of the Biot parameters that are explored during the inversion. By using a realistic parameter space, we are better able to predict the viability of the technique in a real scenario. The system is described by a half-space of water over fluid-saturated sediment. For the inversions that follow, the sound speed and density of the water column are considered known at $c=1530$ m/s and $\rho=1.03$ g/cm^3, respectively. The parameter values used to generate the simulated reflection data are based on nominal values for fluid-saturated sand and are listed in Table I in the column labeled "true." Twelve of the 13 parameters are varied in the inversion. However, in many applications, one or more of these parameters would be known. The limits of the search space for each of the parameters were chosen based on theoretical limits and possible experimental conditions as explained below.

1. Bulk properties

a. Porosity, β: (Limits: 0.26–0.47) Porosity is the ratio of volume of the pores to the total volume of the element. For spheres, a tetrahedral close packing yields a theoretical lower limit of 0.26; a cubic packing gives a value of 0.47,

TABLE I. Biot parameters used to generate the simulated reflection data and bounds on the parameters in the analysis. The pore size is not varied independently in the inversion but is calculated with the Kozeny-Carmen equation, Eq. (7).

Parameter	True	Min.	Max.
ρ_f-g/cm^3	1.03	1.02	1.04
K_f-GPa	2.3	2.0	2.5
η-kg/(m s)	1.0×10^{-3}	1.0×10^{-5}	1.5×10^{-3}
ρ_s-g/cm^3	2.69	2.6	2.7
K_r-GPa	36	32	49
β	0.38	0.26	0.47
τ-m^2	1.35	1.0	3.0
a_p-m	2.67×10^{-5}		
κ-m^2	2.5×10^{-11}	1×10^{-13}	1×10^{-9}
μ-Pa	3.0×10^{7}	1×10^{7}	2×10^{9}
μ_i-Pa	1.0×10^{6}	0	1×10^{8}
K_b-Pa	4.4×10^{7}	1×10^{7}	3.6×10^{8}
$K_{b,i}$-Pa	1.0×10^{6}	0	1×10^{8}

generally considered the upper limit for most sands.

b. Fluid density, ρ_f: (Limits: 1.020–1.040 g/cm^3) The fluid density can vary within small limits due to temperature or salinity. An uncertainty of ±0.020 g/cm^3 is reasonable for experimental conditions found in temperate ocean climates.

c. Fluid bulk modulus, K_f: (Limits: 2.0–2.5 GPa) The fluid bulk modulus is usually measured using the sound speed in the fluid, c, through $c^2=K_f/\rho_f$. An average value for the water sound speed in the ocean is between 1450 and 1530 m/s, giving a fluid bulk modulus between 2.2 and 2.5 GPa. However, it has been suggested that the fluid bulk modulus can also be dependent on the amount of absorbed gas or gas bubbles in the sediment produced by benthic activity.[20] This effect would lower the fluid bulk modulus in the sediment but not in the water column. Therefore, the lower limit of the fluid bulk modulus is set to accommodate up to 3 ppm of gas bubbles that may be produced by residual benthic activity.

d. Grain density, ρ_g: (Limits: 2.6 to 2.7 g/cm^3). The value of ρ_g has been measured for quartz sand at 2.650 g/cm^3 and should vary little when the grain material is uniform.

e. Grain bulk modulus, K_r: (Limits: 32 to 49 GPa) The bulk modulus of quartz is 36 GPa from standard references. In one study, the grain bulk modulus of sand in a laboratory tank was determined from a suspension of sand grains in a liquid with a density matching that of the sand grains using Wood's equation. This measurement produced a 95% confidence interval of 32 to 49 GPa.[21]

2. Fluid flow properties

a. Viscosity, η: [Limits: 1.0×10^{-5}–1.5×10^{-3} kg/(m s)]. The viscosity is found to vary little when measured.[3] The expected value of viscosity of water is $1.0E-3$ kg/(m s) from standard references.

b. Permeability, κ: (Limits: 1×10^{-13} to 1×10^{-9} m^2) Permeability measures quantitatively the ability of a porous medium to conduct fluid flow. By comparing a number of measurement techniques in order to quantify their relative inaccuracies. Taylor-Smith has found that permeability can vary as much as two orders of magnitude depending on the measurement.[19] Also, Taylor-Smith points out that in some cases the Biot model can predict permeabilities that are several orders of magnitude higher than what is measured, while in other cases, the Biot model predicts the same values that are found from direct flow methods. One of the possible explanations may be that permeability is frequency dependent. Although, much of the frequency dependence of the permeability is accounted for within the Biot model through the viscous loss term, some frequency dependence in the permeability can arise from grains which are not part of the frame and are floating. In a high-frequency regime, these grains remain suspended. While in the constant flow regime, these particles would tend to be pushed into pore openings, decreasing the permeability. Therefore, for this study, the permeability is given wide limits.

c. Pore size, a: (Limits: 2×10^{-6}–2×10^{-4} m) The pore size is the size of the pore space between the sand grains. The Kozeny-Carmen equation relates the values of permeability κ, tortuosity τ, porosity β, and pore size a[22]

$$\kappa=\frac{a^2\beta}{8\tau}. \tag{7}$$

For the purposes of this inversion, the pore size was calculated using the Kozeny-Carmen equation.

d. Tortuosity, τ: (Limits: 1–3 m^2) Tortuosity is the square of the ratio of the minimum path length of a contiguous path through the pore network to the straight-line path. For uniform cylindrical pores with axes parallel to the gradient, the tortuosity equals 1, while for a random system of uniform pores with all possible orientations, the theoretical maximum value is 3.

3. Frame properties

a. Frame shear modulus, $\mu+i\mu_i$: (Limits, real part: 1×10^7–2×10^9 Pa; imaginary part: 0–1×10^8 Pa). The frame shear modulus is the resistance of the frame to a tangential deformation, and generally, its value is unknown. However, in an elastic medium the shear wave speed c_s is related to the real part of the frame shear modulus μ by

$$c_s=\sqrt{\frac{\mu}{\rho}}. \tag{8}$$

Although this equation is not entirely valid for the poroelastic case because of the effects of the interstitial fluid, it is useful for determining the order of magnitude of the frame shear modulus. The shear wave speed has been measured between 70 and 147 m/s in sandy sediments at a frequency of 300 Hz to 10 kHZ.[23,24,10,25,26] There are no measurements of the shear wave speeds at the upper end of the frequency range because the high shear attenuation at these frequencies prohibits the measurement. Therefore, a shear wave speed of 1000 m/s will be taken as the upper limit. For a shear wave speed of 90 m/s, the frame shear modulus is 16 MPa. While for a shear wave speed of 1000 m/s, the frame shear modulus is 1.0 GPa. Therefore,

due to lack of knowledge of shear modulus, and the fact that the shear wave speed has not been measured for high frequencies in unconsolidated sediments, this parameter is allowed to vary widely.

Since frictional losses can occur with the deformation of the frame, an imaginary part of the frame shear modulus μ_i is included to account for the deformation and has a value that is related to the shear attenuation. It is difficult to obtain a value for the shear attenuation at high frequency, and data taken in the 1–20-kHz range suggest that the attenuation is not truly linear with frequency.[25] Therefore, large limits are set on μ_i to account for this uncertainty and frequency dependence.

b. Frame bulk modulus $K_b+iK_{b,i}$: (Limits, real part: $1\times10^7-3.6\times10^8$ Pa; imaginary part: $0-1\times10^8$ Pa) The frame bulk modulus is the resistance of the frame to a compressional deformation. The frame bulk modulus of water saturated sand is unknown and is allowed to vary widely.

III. INVERSION METHOD

The overall purpose of the inversion algorithm is to obtain estimates of the unknown parameters required to produce modeled values that best match the data. The elements of the inversion process are (1) the forward model; (2) the cost function used to quantify the match between model and data; and (3) the technique used to search the parameter space.

A. Forward model

For the present work, the OASES (Ocean Acoustics and Seismic Exploration Synthesis) Reflection Coefficient Module (OASR) from the OASES package version 2.1, is the forward model in the inversions. OASES is a collection of programs used to model acoustic propagation in layered fluids and sediments.[27] OASR is the submodule of the OASES analysis package that calculates reflection loss coefficients over a given range of sampling frequencies and grazing angles. In addition, OASR can accommodate both elastic and poroelastic models of the seafloor and its strata. A theoretical description of the reflection model is found in Ref. 28 and generally follows the derivation found in Appendix B of Ref. 7.

B. Optimization

The cost function to be optimized in the inversion quantifies the mismatch between the model and the data. When a perfect match is obtained, the value of the cost function is 1. The inversion attempts to maximize the cost function by adjusting the modeling parameters. The ideal cost function should have a varied landscape with significant gradients to optimize the chance of finding the global maximum.

The cost function considered for this work is a relative, least-squares cost function defined by

$$C(x)=1-\frac{1}{N_f N_{\theta}}\sum_{f,\theta}\left[\frac{R_d(f,\theta)-R_m(f,\theta,\mathbf{x})}{R_m(f,\theta,\mathbf{x})}\right]^2, \tag{9}$$

where $R_d(f,\theta)$ is the magnitude of the reflection coefficients measured at frequency f and grazing angle θ, and $R_m(f,\theta,\mathbf{x})$ are the corresponding modeled values obtained for the set of N parameters in $\mathbf{x}$. Because this is an analytic function, it is expected to have continuous and finite derivatives.

Inversions not only require a quantitative comparison of experimental and modeled data but also a strategy for sampling the N-dimensional parameter search space. To accomplish this task, a simulated annealing (SA) algorithm[29] is used to optimize the cost function. SA searches for the global maximum of the cost function using random perturbations and sequential variation of parameters with probabilistic criteria to accept and reject possible solutions. In this present work, OASR constructs a forward model based on the parameter variations from SA. The SA algorithm terminates when convergence is achieved.

C. Rotated coordinates

To obtain more information about how parameters are coupled to each other and the relative sensitivities of the reflection coefficient to changes in the parameters, rotated coordinates are computed that can be used to navigate the search space in the inversion.[30] The coordinate rotation of the parameter space is defined using the eigenvectors of K, the covariance matrix of derivatives of the cost function with respect to the N individual parameters. The components of K are defined as

$$K_{ij}=\int_{\Omega}\frac{\partial C}{\partial\hat{x}_i}\frac{\partial C}{\partial\hat{x}_j}d\Omega, \tag{10}$$

where $i,j=1,\ldots,N$, and C is the cost function. To effectively compare the parameters in $\mathbf{x}$, the dimensions are removed by dividing each parameter by the difference in the maximum and minimum values: $\hat{x}_i=x_i/(x_{\max i}-x_{\min i})$. Ω defines the bounds on the parameter space. The integration is carried out using Monte Carlo integration techniques.[31]

The N eigenvectors of K are the rotated coordinates and indicate how the parameters are coupled. The rotated coordinates $\mathbf{v}_i$ and the eigenvalues s_i provide information about the relative sensitivities of the cost function to changes in the individual parameters. For example, the rotated coordinate that corresponds to the largest eigenvalue of K defines the most efficient way to increase the cost function. Each rotated coordinate can be used in turn to vary the individual parameters in a fast simulated annealing algorithm[32] as in Ref. 30.

As an example, the rotated coordinates obtained for the Biot parameters, using the simulated reflection data from 0.1–1 kHz, the bounds listed in Table I, and 1200 samples in the Monte Carlo integration, are shown in Fig. 1. Each rotated coordinate, or eigenvector, is plotted as a row in Fig. 1, and the displacement of each circle from the dotted line indicates the amplitude of the element in the eigenvector corresponding to each parameter. The rotated coordinates have been sorted according to the eigenvalues, shown in Fig. 2. The eigenvalues are scaled by the largest eigenvalue and plotted on a logarithmic scale. In the first rotated coordinate, the top line in Fig. 1, the real part of the frame shear modulus, μ, and the real part of the frame bulk modulus have the largest amplitudes. Thus, over the bounds specified in Table I, the most effective way to increase the cost function for this

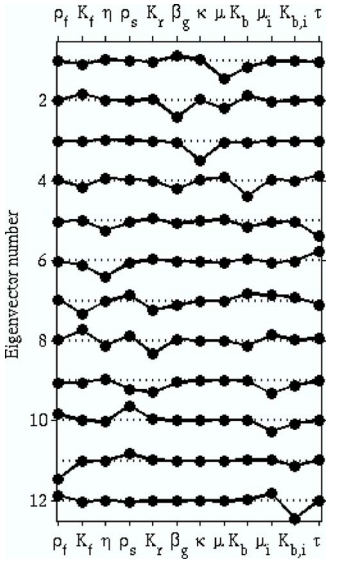

FIG. 1. Rotated coordinates for 12 of the Biot parameters calculated with the bounds shown in Table I for reflection data with frequencies 0.1–1 kHz.

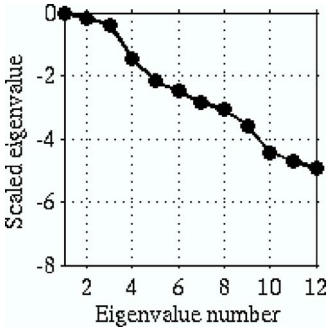

FIG. 2. Eigenvalues associated with the rotated coordinates in Fig. 1. The scaled eigenvalues are the ratios of each eigenvalue to the largest on a log scale.

frequency band is to change μ and K_b in the ratio indicated. The second rotated coordinate reveals coupling between the porosity, β, and the frame shear modulus. The third rotated coordinate has a large component from the permeability, κ. In the fourth rotated coordinate, the porosity, β, the real part of the frame bulk modulus and the fluid bulk modulus have contributions. The tortuosity has a large component in the fifth rotated coordinate. The sixth rotated coordinate is dominated by the viscosity, η, and the tortuosity, τ. The remaining rotated coordinates can be interpreted in the same manner. Every parameter is represented in at least one of the rotated coordinates. Parameters that only have large amplitudes in the higher order rotated coordinates, especially those which correspond to eigenvalues that are three orders of magnitude or more smaller than the largest eigenvalue, do not influence the cost function significantly as they are varied over the bounds Ω.

It is important to remember that the eigenvalues and rotated coordinates can be highly dependent on the bounds on the integration Ω in Eq. (10). For example, the limits on the well-known parameters, such as densities of the fluid and grains, are very small. Thus, varying these parameters within these limits has very little effect on the forward model, and the rotated coordinates. Therefore, the rotated coordinates with large amplitudes for those parameters are associated with much smaller eigenvalues.

IV. RESULTS

The simulated reflection data are analyzed in four ways. (1) The sensitivity of each parameter is determined by computing the rotated coordinates which indicate which parameters most influence the cost function over the specified bounds. (2) The accuracy of the parameter estimates is determined by comparison to the true values. (3) The precision of the inversion results is investigated by considering scatter plots of the accepted parameter values versus the the associated cost functions values. (4) The ability of the parameter estimates to predict broadband acoustic behavior is evaluated by comparing the predicted broadband compressional sound speed, attenuation, normal reflection coefficient, and shear speed.

A. Parameter sensitivity

Rotated coordinates are calculated separately for each decade of the frequency band 100 Hz to 1 MHz. The results of the sensitivity analysis are presented in Tables II–V. Parameters are ranked from most sensitive (MS) to least sensi-

TABLE II. Parameters estimates and sensitivities obtained from simulated annealing inversions for the 100-Hz to 1-kHz frequency band.

Parameter	Estimate	Sensitivity	Accuracy	Precision	Couplings
ρ_f-g/cm^3	1.031	LS	0.09%	NB	
K_f-GPa	2.23	MS (2,4)	3%	LB,UB	μ, β
η-kg/(m s)	0.788×10^{-3}	S(5,6)	21%	LB	
ρ_s-g/cm^3	2.67	LS	0.8%	UB, LB	
K_r-GPa	39.8	LS	10%	LB	
β	0.372	MS(2,4)	2%	LB, UB	μ, K_f
τ	1.32	S(5,6)	21%	LB, UB	η
κ-m^2	1.97×10^{-11}	MS(3)	21%	UB	
μ-Pa	3.0×10^{7}	MS(1,2)	0%	UB	K_b
μ_i-Pa	1.0×10^{6}	LS	0%	LB, UB	
K_b-Pa	4.33×10^{7}	MS(1,4)	2%	UB	μ
$K_{b,i}$-Pa	9.5×10^{6}	LS	850%	UB	

TABLE III. Parameters estimates and sensitivities obtained from simulated annealing inversions for the 1–10-KHz frequency band.

Parameter	Estimate	Sensitivity	Accuracy	Precision	Couplings
ρ_f–g/cm^3	1.020	LS	0.9%	NB	
K_f–GPa	2.05	MS(3,5,6)	11%	UB	
η–kg/(m s)	0.821×10^{-3}	LS	17%	LB	
ρ_s–g/cm^3	2.67	LS	3%	LB, UB	
K_r–GPa	43.4	LS	20%	LB	
β	0.342	MS(3,5,6)	10%	UB, LB	μ, μ_i
τ	1.25	S(4,5,6)	7%	LB, UB	
κ–m^2	2.01×10^{-11}	MS(2)	19%	UB	
μ–Pa	3.0×10^{7}	MS(1,4,5,6)	2%	UB, LB	β, μ_i
μ_i–Pa	1.0×10^{6}	S	0%	LB, UB	β, μ
K_b–Pa	4.48×10^{7}	S(6)	2%	UB, LB	
$K_{b,i}$–Pa	1.38×10^{6}	LS	38%	UB	

tive (LS) in the following manner. If the parameter has a significant magnitude in the first three eigenvectors, it is considered most sensitive (MS). If it is only represented in the fourth through sixth eignevector it is considered sensitive (S). If a parameter does not have a contribution in the first six eigenvectors it is considered least sensitive (LS). For the parameters from the first five eigenvectors, the eigenvector number is also annotated.

Also, some parameters are coupled as described in Sec. III C. The parameter couplings are provided in the column "couplings."

From Tables II–V, the inversion should obtain good estimates for the fluid bulk modulus K_f, porosity β, permeability κ, and frame shear and bulk moduli μ and K_b, respectively, for the lowest two frequency bands with less sensitivity for the frame bulk modulus as the frequency increases. Above 100 kHz, the inversion is less sensitive to the permeability while the dependence on the tortuosity increases. This is due to permeability being one of the major parameters affecting the transition region on the dispersion which is strongest in the 100 Hz–100-kHz region. (See Fig. 4.)

Although the inversion is sensitive to many parameters, estimating their value may be difficult due to coupling. For example, although there is a contribution of the fluid bulk modulus K_f, in many of the rotated coordinates, estimation of its values in this manner may prove difficult. This type of coupling may cause inaccuracies both in the estimation of K_f and β.

Lastly, as described in Sec. III C, the sensitivities calculated are dependent upon both the underlying model and the bounds chosen for the parameters. Therefore, these results should be used to determine of the viability of the entire technique rather than to gain insight of the coupling of parameters within the Biot model.

B. Accuracy of parameter estimates

The accuracy of the parameter estimates is determined by comparing the inversion results to the real values and computing the relative error as shown in Tables II–V. As seen in the tables, generally good estimates are obtained for the most sensitive parameters with a few exceptions. For example, in the highest frequency band, estimates for the porosity and tortuosity are less accurate due to the coupling between these parameters.

The inversion provides a good estimate of the porosity, fluid bulk modulus, and frame shear modulus over the entire band. Permeability estimates are good in the lower frequencies where the influence of the dispersion transition is appar-

TABLE IV. Parameters estimates and sensitivities obtained from simulated annealing inversions for the 10-100-kHz frequency band.

Parameter	Estimate	Sensitivity	Accuracy	Precision	Couplings
ρ_f-g/cm^3	1.0387	LS	0.8%	NB	
K_f-GPa	2.36	MS(2,6)	3%	LB, UB	β, K_b
η-kg/(m s)	3.6×10^{-4}	LS	63%	LB, UB	
ρ_s-g/cm^3	2.70	LS	0.3%	NB	
K_r-GPa	45.4	LS	26%	LB	
β	0.399	MS(2,3)	5%	LB, UB	K_f, τ, K_b
τ	1.45	MS(3,4)	7%	LB, UB	β, K_b
κ-m^2	0.759×10^{-11}	S	69%	UB	
μ-Pa	2.86×10^{7}	MS(1)	5%	LB, UB	
μ_i-Pa	1.08×10^{6}	LS	8%	LB, UB	
K_b-Pa	2.74×10^{7}	MS(2,3,4,6)	37%	UB	K_f, β, τ
$K_{b,i}$-Pa	2.04×10^{6}	LS	104%	UB	

TABLE V. Parameters estimates and sensitivities obtained from simulated annealing inversions for the 100-kHz–1-KHz frequency band.

Parameter	Estimate	Sensitivity	Accuracy	Precision	Couplings
ρ_f-g/cm^3	1.034	LS	0.3%	NB	
K_f-GPa	2.50	MS(2,6)	9%	LB	β, K_b
η-kg/(m s)	1.5×10^{-4}	LS	48%	LB	
ρ_s-g/cm^3	2.62	LS	3%	UB	
K_r-GPa	48	LS	33%	LB	
β	0.427	MS(2,3,4)	12%	LB, UB	K_f, τ, K_b
τ	2.05	MS(3,4)	51%	LB, UB	β
κ-m^2	0.923×10^{-11}	S(5)	63%	UB	
μ-Pa	2.29×10^7	MS(1)	23%	UB	
μ_i-Pa	0.581×10^6	LS	481%	LB, UB	
K_b-Pa	6.28×10^7	MS(2,3,4,6)	42%	LB, UB	K_f, β, τ
$K_{b,i}$-Pa	5.03×10^6	LS	403%	UB	

ent in the reflection coefficient. As the inversion becomes less sensitive to permeability in the upper frequencies, the estimate is also less accurate. Lastly, the estimate for tortuosity is accurate in the midfrequencies where it is sensitive but less accurate in the highest frequency band where it is strongly coupled with the porosity. This coupling also decreases the accuracy of the porosity estimate for the band.

C. Precision of parameter estimates

The precision of the parameter estimates can be determined by plotting each of the parameter estimates in the inversion model versus the cost function value. The estimates listed in Tables II–V occur at the highest cost function value. In order to reduce clutter on the scatter plots, an envelope is drawn to encompass all the highest values of the cost function as illustrated in Fig. 3. Additionally, a dashed vertical line is plotted at the correct value of the parameter.

Three parameters from the inversion, grain density ρ_s, porosity β, and permeability κ, are shown for the four frequency bands. The lowest frequency band is indicated by the lightest line and the highest by the darkest with increasing shades in between. A flat or wide envelope as with the grain density shown in Fig. 3(a) reveals that, even though the inversion returns an estimate for the parameter, the uncertainty associated with the estimate is essentially equivalent to the bounds on the parameter. For the data employed in the inversion, a parameter such as the one represented in Fig. 3(a) has no effect on the reflectivity when varied over these bounds. A tight envelope about the final inverted value indicates a well-determined parameter as in Fig. 3(b). As seen in the figure, the porosity estimates has both an upper and lower bound and is well defined. Note also that, although porosity is precisely determined for the highest band of frequencies, the estimate is not accurate. This is due to the coupling of porosity with other parameters such as tortuosity as described in the previous section. Lastly, a parameter may only have a lower or upper bound as illustrated with the permeability in Fig. 3(c).

Tables II–V summarize the precision of each parameter. "NB" indicates no bound as in Fig. 3(a). "LB,UB" indicates that there are both an upper and lower bound present. Lastly, "UB" or "LB" indicate an upper or lower bound as in Fig. 3(c).

Although this is a somewhat simplistic method of determining uncertainties, it provides a qualitative comparision of the reliability of the parameter estimates obtained by the inversion. More rigorous approaches to the problem of estimating uncertainty have been suggested.[33–35] However, these methods have not yet been applied to the Biot model.

There are four key points summarized in Tables II–V. (1) The most precise and accurate parameters as shown by the scatter plots are generally given by the parameters which have a large contribution to eigenvectors associated with the largest eigenvalues. (2) Parameters with very small bounds are generally not sensitive in the inversion. (3) A subset of parameters is sensitive across all frequency bands, namely porosity, fluid bulk modulus, and frame shear modulus. (4) There is a frequency dependence of the sensitivity of the Biot parameters. This is most evident in the permeability, which is sensitive and accurate in the lower frequencies and less sensitive and less accurate in the upper frequencies.

D. Implications for the predictive abilities of reflection coefficient inversion

The parameter estimates obtained from the inversion in each frequency range were used to calculate the broadband

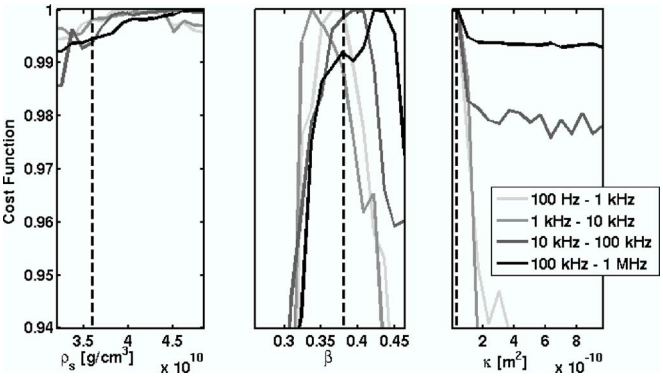

FIG. 3. Envelope plots for the grain density ρ_s, porosity β, and permeability κ for the four frequency bands.

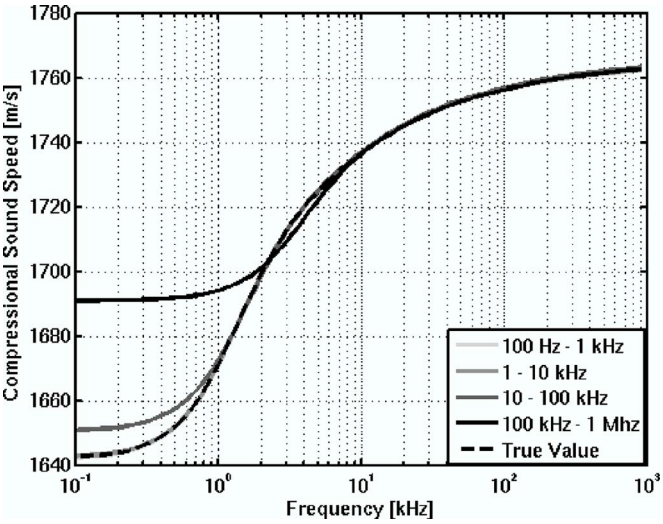

FIG. 4. The compressional sound speed associated with the parameters in Table I and the inversion results in Tables II–V.

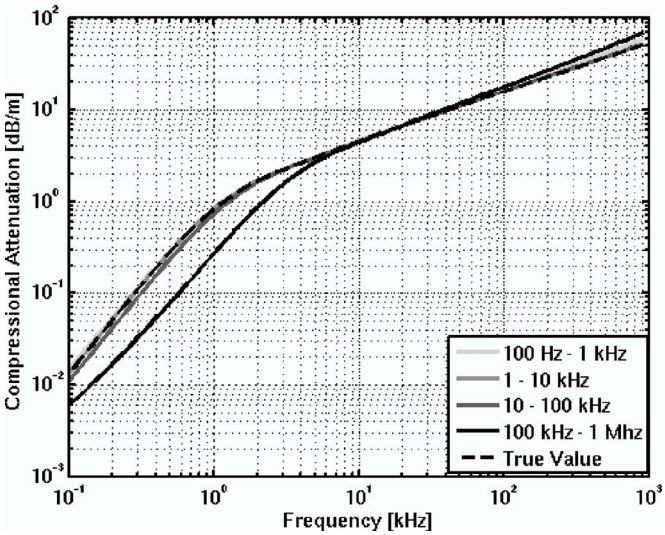

FIG. 5. The compressional attenuation associated with the parameters in Table I and the inversion results in Tables II–V.

compressional sound speed, attenuation, normal reflection coefficient, and shear sound speed. This analysis provides an estimation of the predictive abilities of inversions from particular frequency regimes and indicate which frequency ranges should be measured in order to predict the broadband behavior.

First, consider the dispersion curve in Fig. 4. Inversions from the two lowest frequency decades, 0.1–10 kHz, correctly predict the value and shape of the dispersion curve over the entire four-decade band, while the inversion estimates from the two highest decades do not. At the highest frequency, 100–1000 kHz, shown as the black line, the prediction obtained from the parameter estimates fails to match the values for the low-frequency sound speed and much of the transition region. This implies that inversions based on reflection coefficient measurements taken at high frequencies alone are not sufficient to describe broadband behavior. This is almost entirely due to the poor estimate of permeability. In contrast, inversions from the lower frequencies matched the entire curve very well. Therefore, if reflection coefficient inversions are to be used as a tool for sediment characterization, low-to midfrequency data covering the transition region of the dispersion curve should be used.

Similar results are evident in the attenuation (Fig. 5) and normal reflection coefficient (Fig. 6). It is clear from these figures that inversion based on low-or midfrequency reflection data are adequate to describe the broadband behavior while high-frequency data inversions are not. This is especially evident in the normal reflection coefficient where there is a large drop in the reflectivity over the transition region. The frequency of the nadir of the normal reflection coefficient is highly influenced by the value of the sediment permeability, while the depth of the decrease is dependent on the porosity. Therefore, for the range of frequencies over which the inversion is not sensitive to the permeability, the inversion estimates do not provide a good estimate of the frequency of the decrease, while if the porosity is poorly described the depth of the decrease is not accurate.

Lastly, the inversion estimates are used to predict the broadband shear sound speed. At the outset, good predictions for the shear wave speed were not expected because coupling between the water-borne wave and shear wave were expected to be weak due to the large sound-speed mismatch. However, the frame shear modulus was highly sensitive in the inversion and good estimates for this parameter were obtained. This is due to the influence of the shear wave on the reflection coefficient at low grazing angles. Figure 7 shows the influence of the frame shear modulus at a grazing angle of 3 deg. When the frame shear modulus is at the upper bound, there is significant coupling into the shear mode and the reflection coefficient is greatly affected. However, when the change in frame shear modulus is small, there is a much smaller change in the reflection coefficient that would be difficult to measure in practice. Because of the large effect at high values of the frame shear modulus, good estimates for the shear wave speed were obtained for every frequency band inversion with the lowest frequency bands

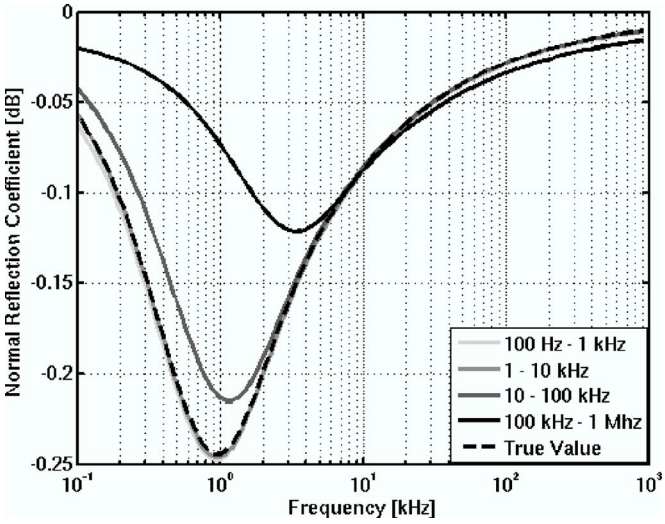

FIG. 6. The normal reflection coefficient associated with the parameters in Table I and the inversion results in Tables II–V.

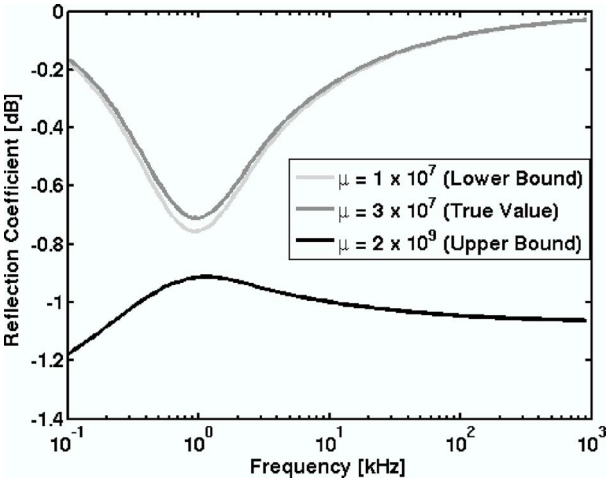

FIG. 7. The effect of the frame shear modulus μ on the value of the low grazing angle (3 deg) reflection coefficient.

the most accurate. (See Fig. 8.) Therefore, the shear wave speed may be predicted using reflection coefficient inversions with decreasing accuracy as frequency increases.

V. CONCLUSIONS

This study sought to determine the ability of parameter estimates obtained from inversions based on reflection data for a limited frequency range to predict broadband behavior. Simulated reflection coefficient data were produced over a large frequency range, 100 Hz to 1 MHz, using the Biot poroelastic model as formulated by Stoll. The data were analyzed in 4 decade regimes, 0.1–1, 1–10, 10–100, and 100–1000 kHz. The results were analyzed with respect to four criteria: (1) The sensitivity of the inversion to each parameter was determined by calculating the rotated coordinates. (2) The accuracy of the inversion was computed by comparing the parameter estimates to the true values. (3) The precision of the estimates was qualitatively determined using scatter plots of the accepted parameter values versus the cost function. (4) The estimates were considered for their ability to predict the broadband acoustic behavior over the broadband.

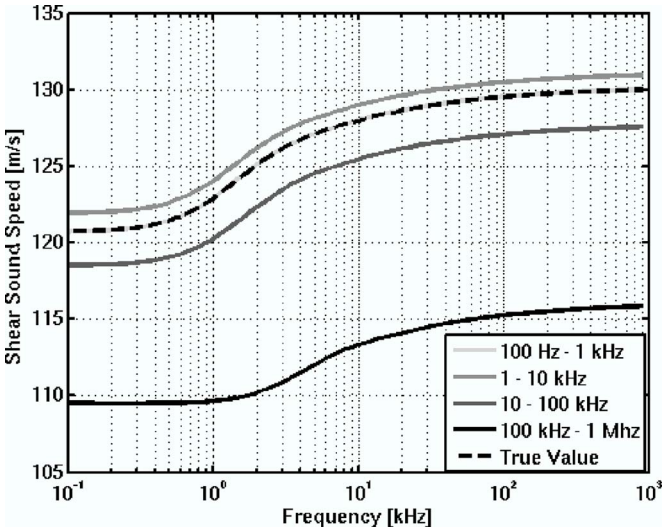

FIG. 8. The shear sound speed associated with the parameters in Table I and the inversion results in Tables II–V.

There are four primary results of this work. First, inversions based on reflection coefficient data give reasonable parameter estimates, especially for the most sensitive parameters. Three parameters were accurately determined for every frequency band: porosity, fluid bulk modulus, and frame shear modulus. Additionally, the lowest two frequency bands give good estimates for the permeability. The predicted accurate estimate of permeability and frame shear modulus demonstrates improvement over the normal reflection coefficient inversion which required additional measurements or interrelational expressions to estimate these quantities.[15] For the highest frequency band, the estimate for porosity is somewhat less accurate due to a coupling with the tortuosity. Since reflection coefficients can be measured noninvasively, there is potential that such inversions could provide a means of characterizing ocean seabeds.

Second, the sensitivity of the reflection coefficient data to the Biot parameters is frequency dependent. This is especially evident in the case of permeability. In the lowest two frequency regimes, in which the dispersion transition is apparent in the reflection coefficient, permeability is highly sensitive and a good estimate for permeability is determined. In contrast, for frequencies above the transition region, permeability is less sensitive and accurate estimates are not obtained.

Third, data taken over a limited high-frequency range may not be able to fully describe broadband acoustic behavior. Inversion results for single-decade frequency bands that included a portion of the low-frequency to high-frequency sound speed transition region successfully predict the dispersion, attenuation, normal reflection coefficient, and shear speed for the entire four-decade band. However, when only frequencies above the transition region were used in the inversion, the resulting parameter estimates were unable to accurately predict the broadband behavior.

Fourth, reasonable estimates of the shear speed were determined using reflection coefficient data. This result was unexpected due to the large speed mismatch of the waterborne sound and the sediment shear wave. However, the frame shear modulus was found to be sensitive due to the influence of the shear speed on low grazing angle reflection data.

Finally, it should be noted that these conclusions are based on inversions from data simulated by a particular realization of the Biot-Stoll model. Significant differences have been noted when comparing the Biot-Stoll model to experimental data,[9] implying a more complicated physical model. Also, experimental data may include effects of interface roughness, volume inhomogeneities, range dependence, layering, and other experimental effects. The influence of these effects on the inversion will be explored in subsequent publications.

ACKNOWLEDGMENTS

The authors would like to thank the Office of Naval Research and Robert Headrick for sponsoring this work.

Thanks also to Dr. Nicholas Chotiros for many helpful discussions. Lastly, thanks for Dr. Henrik Schmidt and Dr. Morris Stern, who developed the OASES code which was the basis of the forward model.

[1]N. Chotiros, "Inversion and sandy ocean sediment," in *Full Field Inversion Methods in Ocean and Seismic Acoustics*, Transport Processes in Porous Media edited by A. Caiti, P. Gerstoft, and H. Schmidt (Kluwer Academic, Dordrecht, 1995).
[2]M. Isakson and T. Neilsen, "A comparison of elastic and poro-elastic models for inversions of reflection loss measurements of a smooth water/sand interface at high frequencies," in *Acoustic Inversion Methods and Experiments for the Assessment of the Shallow Water Environment* (Kluwer Academic, Dordrecht, in press).
[3]K. Williams, D. Jackson, E. Thorsos, D. Tang, and S. Schock, "Comparison of sound speed and attenuation measured in a sandy sediment to predictions based on the Biot theory of porous media," IEEE J. Ocean. Eng. **27**, 413–428 (2002).
[4]T. Yamamoto and A. Turgut, "Acoustic wave propagation through porous media with arbitrary pore size distributions," J. Acoust. Soc. Am. **83**, 1744–1751 (1988).
[5]J. Tatersall and D. Chizhik, "Application of biot theory to the study of acoustic reflection from sediments," in *Technical Report* NUWC-NLTR-10-115 (Naval Undersea Warfare Center, New London, 1992).
[6]M. Biot, "Theory of propagation of elastic waves in a fluid saturated porous solid. II. Higher frequency range," J. Acoust. Soc. Am. **28**, 179–191 (1956).
[7]R. Stoll, *Sediment Acoustics, Lecture Notes in Earth Science* (Springer, Berlin, 1983).
[8]K. Williams, "An effective density fluid model for acoustic propagation in sediments derived from Biot theory," J. Acoust. Soc. Am. **110**, 2276–2281 (2001).
[9]N. Chotiros and M. Isakson, "A broadband model of sandy ocean sediments: Biot-Stoll with contact squirt flow and shear drag," J. Acoust. Soc. Am. **116**, 2011–2022 (2004).
[10]M. Richardson, K. Briggs, L. Bibee, P. Jumars, W. Sawyer, D. Albert, R. Bennett, T. Berger, M. Buckingham, N. Chotiros, P. Dahl, N. Dewitt, P. Fleischer, R. Flood, C. Greenlaw, D. Holliday, M. Hulbert, M. Hutnak, P. Jackson, J. Jaffe, H. Johnson, D. Lavoie, A. Lyons, C. Martens, D. McGehee, K. Moore, T. Orsi, J. Piper, R. Ray, A. Reed, R. Self, J. Schmidt, S. Schock, F. Simonet, R. Stoll, D. Tang, D. Thistle, E. Thorsos, D. Walter, and R. Wheatcroft, "Overview of SAX99: Environmental considerations," IEEE J. Ocean. Eng. **26**, 26–51 (2001).
[11]N. Chotiros, "An inversion for biot parameters in water-saturated sand," J. Acoust. Soc. Am. **112**, 1853–1868 (2002).
[12]C. Harrison, "Noise modeling, noise experiment and noise inversion," J. Acoust. Soc. Am. **118**, 1844–1845 (2005).
[13]C. Holland and B. Brunson, "The Biot-Stoll sediment model: an experimental assessment," J. Acoust. Soc. Am. **84**, 1437–1531 (1998).
[14]C. Holland, J. Dettmer, and S. Dosso, "Remote sensing of sediment density and velocity gradients in the transition layer," J. Acoust. Soc. Am. **118**, 163–177 (2005).
[15]S. Schock, "A method for estimating the physical and acoustic properties of the sea bed using chirp sonar data," IEEE J. Ocean. Eng. **29**, 1200–1217 (2004).
[16]M. Clennell, "Tortuosity: A guide through the maze," in *Developments in Petrophysics, Geo. Soc. Special Pub. 122*, edited by M. Lovell and P. Harvey (Geo. Soc., London, U.K., 1997).
[17]F. Dullien, *Porous Media, Fluid Media and Pore Structure* (Academic, San Diego, CA, 1992).
[18]S. Forster, B. Bobertz, and B. Bohling, "Permeability of sands in the coastal areas of the Southern Baltic Sea: Mapping a grain-size related sediment property," Aquat. Geochem. **9**, 171–190 (2003).
[19]D. Taylor-Smith, "Geophysical-geotechnical predictions," in *Shear Waves in Marine Sediments*, edited by J. Hovem, M. Richardson, and R. Stoll (Kluwer Academic, Dordecht, 1993), pp. 725–734.
[20]R. Stoll, "Velocity dispersion in water-saturated granular sediment," J. Acoust. Soc. Am. **111**, 785–793 (2002).
[21]M. Richardson, K. Williams, K. Briggs, and E. Thorsos, "Dynamic measurement of sand grain compressibility at atmospheric pressure: Acoustic applications," IEEE J. Ocean. Eng. **27**, 593–601 (2002).
[22]P. Carmen, *Flow of Gases through Porous Media* (Academic, New York, 1956).
[23]B. Luke, *In situ measurement of stiffness profiles in the seafloor using the spectral-analysis-of-waves (SASW) method* (Technical Report under ARL:UT Independent Research and Development Program, Austin, TX) (1995).
[24]K. Briggs, "Comparison of measured compressional and shear wave velocity values with predictions from biot theory," in *Shear Waves in Marine Sediments*, edited by J. Hovem, M. Richardson, and R. Stoll (Kluwer Academic, Dordecht, 1991), pp. 121–130.
[25]B. Brunson, "Shear wave attenuation in unconsolidated laboratory sediments," in *Shear Waves in Marine Sediments*, edited by J. Hovem, M. Richardson, and R. Stoll (Kluwer Academic, Dordecht, 1991), pp. 141–148.
[26]D. W. Bell and D. J. Shirley, "Temperature variation of the acoustical properties of laboratory sediments," J. Acoust. Soc. Am. **68**, 227–231 (1980).
[27]H. Schmidt, *OASES Version 2.1 User Guide and Reference Manual* (Department of Ocean Engineering, Massachusetts Institute of Technology, Cambridge, MA, 1997).
[28]M. Stern, A. Bedford, and H. Millwater, "Wave reflection from a sediment layer with depth-dependent properties," J. Acoust. Soc. Am. **77**, 1,781–1,788 (1985).
[29]W. Goffe, G. Ferrier, and J. Rogers, "Global optimization of statistical functions with simulated annealing," J. Econometr. **60**, 65–99 (1994).
[30]M. Collins and L. Fishman, "Efficient navigation of parameter landscapes," J. Acoust. Soc. Am. **98**, 1637–1644 (1995).
[31]W. W. H. Press, A. Teukolsky, W. Vetterling, and B. Flannery, *Numerical Recipes in FORTRAN: The Art of Scientific Computing* (Cambridge University Press, Cambridge, U.K., 1992).
[32]H. Szu and R. Hartley, "Fast simulated annealing," Phys. Lett. A **122**, 157–162 (1987).
[33]S. Jaschke and N. Chapman, "Matched field inversion of broadband data using the freeze bath method," J. Acoust. Soc. Am. **106**, 1838–1851 (1999).
[34]S. Dosso and P. L. Neilsen, "Quantifying uncertainty in geoacoustic inversion. II. Application to broadband, shallow-water data," J. Acoust. Soc. Am. **111**, 143–159 (2002).
[35]S. Dosso, "Quantifying uncertainty in geoacoustic inversion. I. A fast Gibbs sampler approach," J. Acoust. Soc. Am. **111**, 129–142 (2002).